







## Article

# Nanocomposite PVDF/TiO<sub>2</sub> Photocatalytic Membranes for Micropollutant Removal in Secondary Effluent

Juan C. Aldana <sup>1</sup>, Marta Pedrosa <sup>2,3</sup>, Adrián M. T. Silva <sup>2,3</sup>, Joaquim L. Faria <sup>2,3</sup>, Juan L. Acero <sup>1</sup>  
and Pedro M. Álvarez <sup>1,\*</sup>

- <sup>1</sup> Departamento de Ingeniería Química y Química Física, Instituto Universitario de Investigación del Agua, Cambio Climático y Sostenibilidad (IACYS), Universidad de Extremadura, Avenida de Elvas s/n, 06006 Badajoz, Spain; aldana@unex.es (J.C.A.); jlacero@unex.es (J.L.A.)
- <sup>2</sup> LSRE-LCM—Laboratory of Separation and Reaction Engineering—Laboratory of Catalysis and Materials, Faculty of Engineering, University of Porto, Rua Dr. Roberto Frias, 4200-465 Porto, Portugal; mfpedrosa@fe.up.pt (M.P.); adrian@fe.up.pt (A.M.T.S.); jlfaria@fe.up.pt (J.L.F.)
- <sup>3</sup> ALiCE—Associate Laboratory in Chemical Engineering, Faculty of Engineering, University of Porto, Rua Dr. Roberto Frias, 4200-465 Porto, Portugal
- \* Correspondence: pmalvare@unex.es

**Abstract:** In this study, a mixed-matrix method was used to prepare PVDF polymeric membranes with different amounts of TiO<sub>2</sub> P25 photocatalyst embedded, which were employed in filtration processes in the presence of UV radiation (LED, peak emission at 375 nm) to eliminate two aqueous micropollutants (MPs) used as model compounds (venlafaxine and metoprolol). The obtained membranes were characterized to gain insights into their texture, morphology, composition, and other catalyst-related properties that could affect the photocatalytic filtration process. For that purpose, N<sub>2</sub> adsorption–desorption, contact angle, SEM-EDX, thermal analysis, FTIR, XPS, UV-vis DRS, and PL spectroscopy were used. Filtration tests were carried out in continuous mode using a dead-end filtration cell to evaluate the performance of the prepared membranes in removing the selected MPs. Experiments were performed both in ultrapure water and a secondary effluent from a municipal wastewater treatment plant. It was found that the synthesized membranes could effectively remove the target MPs in ultrapure water, achieving up to 99% elimination. Such process performance decreased drastically in the secondary effluent with removals below 35%. Carbonate/bicarbonate ions in the secondary effluent were identified as the main scavenging substances. Thus, after the partial removal of carbonate/bicarbonate ions from the secondary effluent, the removal of MPs achieved was above 60%.

**Keywords:** membrane; metoprolol; micropollutant; photocatalysis; titania; venlafaxine; wastewater



**Citation:** Aldana, J.C.; Pedrosa, M.; Silva, A.M.T.; Faria, J.L.; Acero, J.L.; Álvarez, P.M. Nanocomposite PVDF/TiO<sub>2</sub> Photocatalytic Membranes for Micropollutant Removal in Secondary Effluent. *Catalysts* **2024**, *14*, 109. <https://doi.org/10.3390/catal14020109>

Academic Editors: Sylwia Mozia and Raffaele Molinari

Received: 29 December 2023

Revised: 18 January 2024

Accepted: 24 January 2024

Published: 28 January 2024



**Copyright:** © 2024 by the authors. Licensee MDPI, Basel, Switzerland. This article is an open access article distributed under the terms and conditions of the Creative Commons Attribution (CC BY) license (<https://creativecommons.org/licenses/by/4.0/>).

## 1. Introduction

The control of micropollutants of emerging concern (MPs) in wastewater treatment plants (WWTPs) is one of the major water challenges today [1]. Household and industrial activities as well as agricultural practices release several classes of MPs into the water, including polar pesticides, perfluorinated compounds, personal hygiene products, and drugs, which can act as endocrine disruptors and may have harmful effects on fertility, growth, metabolism, and hormones [2]. The occurrence of MPs has been repeatedly reported in effluents from WWTPs as well as in both surface water and groundwater, their concentration levels depending on the location and weather conditions [3]. Policymakers show great concern about this issue. Thus, in the last decade, the European Union has developed some control procedures, such as the Commission Implementing Decision (EU) 2022/1307, establishing a watch list of substances to be monitored in water bodies. Also, the European Council is likely to launch a new directive for more efficient treatment of urban wastewater, including a compulsory advanced treatment (i.e., quaternary treatment)

in WWTPs of over 100,000 population equivalent to remove a broad spectrum of MPs. Accordingly, the impact of quaternary treatments on the removal of specific MPs is now a major research topic [4]. In this work, the removal of two MPs chosen as model pollutants, the antidepressant venlafaxine (VEN) and the  $\beta$ -blocker metoprolol (MTP), by PVDF/TiO<sub>2</sub> photocatalytic membranes is studied.

VEN (see Figure 1a) has been often detected in the aquatic environment [5]. In terms of fate, venlafaxine and its metabolites pose serious ecotoxicological risks to aquatic ecosystems, being hardly removed in conventional WWTPs [6,7]. In addition, the long-term effects of its metabolites have not been systematically studied [6]. Likewise, MTP (see Figure 1b) is a persistent MP with potential ecotoxicological threat to aquatic ecosystems [8].

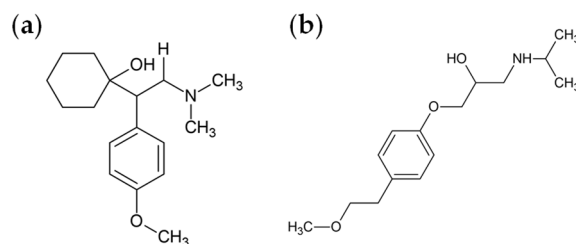


**Figure 1.** Molecular structure of (a) VEN and (b) MTP.

Photocatalysis has emerged recently as a promising green technology to remove MPs from water. Thus, several semiconductor oxides such as TiO<sub>2</sub>, ZnO, ZrO<sub>2</sub>, WO<sub>3</sub>, and Fe<sub>2</sub>O<sub>3</sub>, as well as some carbonaceous materials such as graphene oxide or g-C<sub>3</sub>N<sub>4</sub>, have been widely explored for this purpose, both as single and composite photocatalysts [9,10]. Among them, commercial TiO<sub>2</sub> P25 nanoparticles have been extensively studied in water treatment because of their efficiency in removing MPs, non-toxicity, stability, and low cost [11]. TiO<sub>2</sub> P25 has been reported to be a mesoporous material (60.8 m<sup>2</sup>·g<sup>−1</sup>) composed of irregular shape nanoparticles of sizes largely distributed from 15 to 25 nm and a mean pore size of 17.8 nm [12]. Its band-gap energy of about 3.2 eV makes it suitable to absorb UVA radiation in solar detoxification processes [9]. However, a critical limitation reported for this powdered material is its inability to form stable agglomerates, which could be easily recovered and reused after the treatment [13]. For this reason, different strategies have been proposed to immobilize TiO<sub>2</sub> P25 onto a variety of materials, thus allowing for the photoreactor to operate in a continuous mode [14,15] or the easy recovery of the photocatalyst after its use in batch reactor configurations [16,17]. In this work, TiO<sub>2</sub> P25 nanoparticles have been immobilized onto the structure of a polyvinylidene fluoride (PVDF) membrane to couple the benefits of membrane filtration and TiO<sub>2</sub> photocatalytic oxidation in the removal of MPs from water.

PVDF membranes are prominently used in ultrafiltration owing to their mechanical strength, thermal stability, good chemical resistance, and low cost [18]. Although pristine PVDF membranes have shown high efficiency in removing many MPs from water, the control of membrane fouling and post-treatment of the retentate stream remain challenging [19]. Decoration of filtration membranes with a photocatalyst (i.e., photocatalytic composite membranes) is a promising strategy to overcome these limitations and improve the overall process performance [20]. Photocatalytic membranes combine the sieving function of a polymer-based membrane with a photocatalyst that absorbs radiation to generate reactive oxygen species (ROS), which can effectively degrade MPs on the membrane surface and the water bulk into harmless or less toxic molecules. This synergistic effect allows for minimizing membrane fouling, thus increasing the permeate flux, and reducing the accumulation of MPs in the retentate, requiring a less intensive post-treatment [9].

The photocatalyst (e.g., TiO<sub>2</sub>) can be immobilized onto the membrane by different methods that can be classified as the physical coating, self-assembly, and mixed-matrix method [21]. In the latter, the photocatalyst is blended with the polymeric solution before casting [21]. Recent studies have shown that PVDF/TiO<sub>2</sub> membranes synthesized by

blending methods are effective in reducing fouling [22,23], leading to full recovery of the membrane permeate flux. Synthetic dyes have also been properly removed by PVDF/TiO<sub>2</sub> treatment in batch mode (no filtration system) [24,25]. Moreover, the decoration of TiO<sub>2</sub> with Ag improved the antimicrobial properties, self-cleaning effect, and permeability [26]. Similarly, the immobilization of g-C<sub>3</sub>N<sub>4</sub> onto PVDF membranes has led to enhanced MP removal and anti-fouling properties using visible light [27–30]. PVDF/TiO<sub>2</sub> membranes prepared by using a physical coating have also been demonstrated as being beneficial for the removal of aqueous MPs [9,31]. Thus, for example, Dekkouche et al. achieved up to 94% removal of diclofenac and 17 $\alpha$ -ethinylestradiol using a PVDF/TiO<sub>2</sub> membrane in the continuous filtration mode while keeping high permeability [32]. A cross-flow filtration system proposed by Liu et al. using TiO<sub>2</sub> immobilized onto a PVDF membrane led to >95% removal of 17 $\beta$ -estradiol in the continuous mode [33].

Despite the number of papers published so far on PVDF/TiO<sub>2</sub> membranes for the removal of MPs from water, most of them are focused on their anti-fouling properties and performed MPs removal tests in a batch configuration. Therefore, there is still a gap in the research regarding the performance of photocatalytic filtration systems in more realistic conditions, testing lab-scale continuous-mode membrane reactors for the elimination of MPs. Additionally, more studies are needed to investigate the performance of photocatalytic membranes treating real water matrices as WWTP secondary and tertiary effluents. Consequently, this work focuses on the preparation of PVDF/TiO<sub>2</sub>-P25 membranes via a mixed-matrix method, their characterization, and use in continuous filtration experiments aimed to eliminate VEN and MTP as probe MPs from UP water and a secondary effluent from a WWTP.

## 2. Results and Discussion

### 2.1. Membrane Characterization

A PVDF membrane and a series of photocatalytic membranes (labeled as PVDF-P25-1, PVDF-P25-5, and PVDF-P25-8) were prepared by a mixed-matrix method (described in Section 3.2) and characterized using several techniques. Table 1 shows the BET surface area, pore volume, water contact angle, and thickness of some membrane samples. Figure 2 depicts the N<sub>2</sub> adsorption–desorption isotherms and the BJH pore size distribution of the synthesized membranes. The typical shape of a type-IV isotherm (H3 hysteresis loop) according to the IUPAC classification can be observed for all the samples. This implies that the membranes exhibit very low micropores filling at low relative pressures and behave mainly as macro- and mesoporous adsorbents. From Table 1, it is apparent that inserting TiO<sub>2</sub> P25 into the PVDF membrane brought about a moderate increase in the BET surface area and porosity, likely due to the contribution of the area of the catalyst nanoparticles embedded in the membrane structure [34,35]. However, blending TiO<sub>2</sub> with the membrane has been reported to not significantly affect the typical structure and porosity of PVDF membranes [9].

**Table 1.** BET surface area, pore volume, water contact angle, and thickness of the membranes synthesized in this work.

Membrane	Specific Surface Area (m <sup>2</sup> ·g <sup>−1</sup> )	Pore Volume (cm <sup>3</sup> /g)	Water Contact Angle (°)	Membrane Thickness (μm)
PVDF	11.5	0.025	67.2 ± 3.6	312.8 ± 4.7
PVDF-P25-1	12.4	0.031	66.3 ± 3.1	389.1 ± 6.0
PVDF-P25-5	15.0	0.039	66.6 ± 4.8	180.6 ± 3.6
PVDF-P25-8	14.1	0.036	67.6 ± 1.6	184.5 ± 4.2

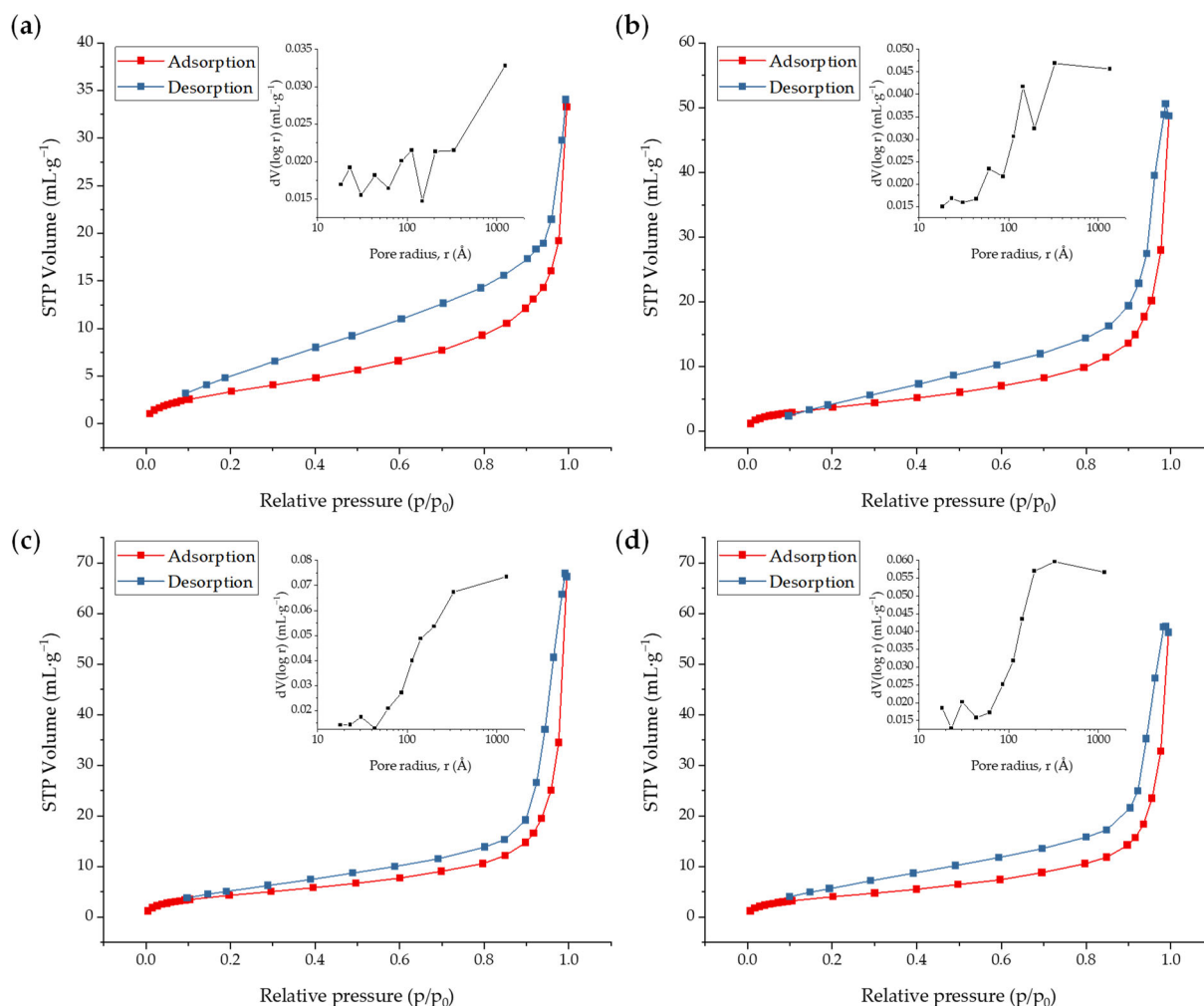


**Figure 2.** Nitrogen BET adsorption–desorption isotherm and pore size distribution determined by the BJH approach from the BET adsorption–desorption isotherms of (a) PVDF, (b) PVDF-P25-1, (c) PVDF-P25-5, and (d) PVDF-P25-8 membranes.

The water contact angle (WCA) provides information about the wetting property of a membrane. Generally speaking, if the WCA is lower than 90°, the membrane surface is considered hydrophilic, while for a larger WCA, the membrane is regarded as hydrophobic. As it can be seen in Table 1, all the prepared membranes have water contact angles of about 67°, typical of slightly hydrophilic surfaces. Although PVDF is regarded as a hydrophobic material, the use of polyvinylpyrrolidone (PVP) for the synthesis of the membrane improved the surface hydrophilicity of the final product [36]. In agreement with this result, a previous work using a similar synthesis method gave rise to a PVDF membrane with a water contact angle of 64° [27]. Usually, the incorporation of TiO<sub>2</sub> into a PVDF membrane improves hydrophilicity due to the increase in surface hydroxyl groups [32,37,38], though some authors claim that below 15 wt.% TiO<sub>2</sub> the increase in hydrophilicity is expected to be small [39]. In our case, no effect of TiO<sub>2</sub> on the water contact angle was observed, which may be due to a low concentration of surface TiO<sub>2</sub> as shown in the XPS analysis (see discussion below).

The morphology of the PVDF/TiO<sub>2</sub> samples showing TiO<sub>2</sub> P25 dispersion and the cross-section structure of the membranes is depicted in Figure 3. First, it can be said that the TiO<sub>2</sub> P25 nanoparticles were evenly distributed in the PVDF-P25 samples, though in the PVDF-P25-1 sample the TiO<sub>2</sub> snowflake agglomerates can be observed, likely due to an inefficient dispersion during the synthesis process. Also, changes in the porosity were observed. While pristine PVDF showed a microstructure with finger-like macropores, the



incorporation of  $\text{TiO}_2$  led to a decrease in pore sizes, thus conferring a more mesoporous-like structure to the membrane. The thickness of the membrane was also affected by the presence of  $\text{TiO}_2$ . Thus, at a high  $\text{TiO}_2$  loading, the thickness decreased drastically, which is in agreement with that observed by others [35].

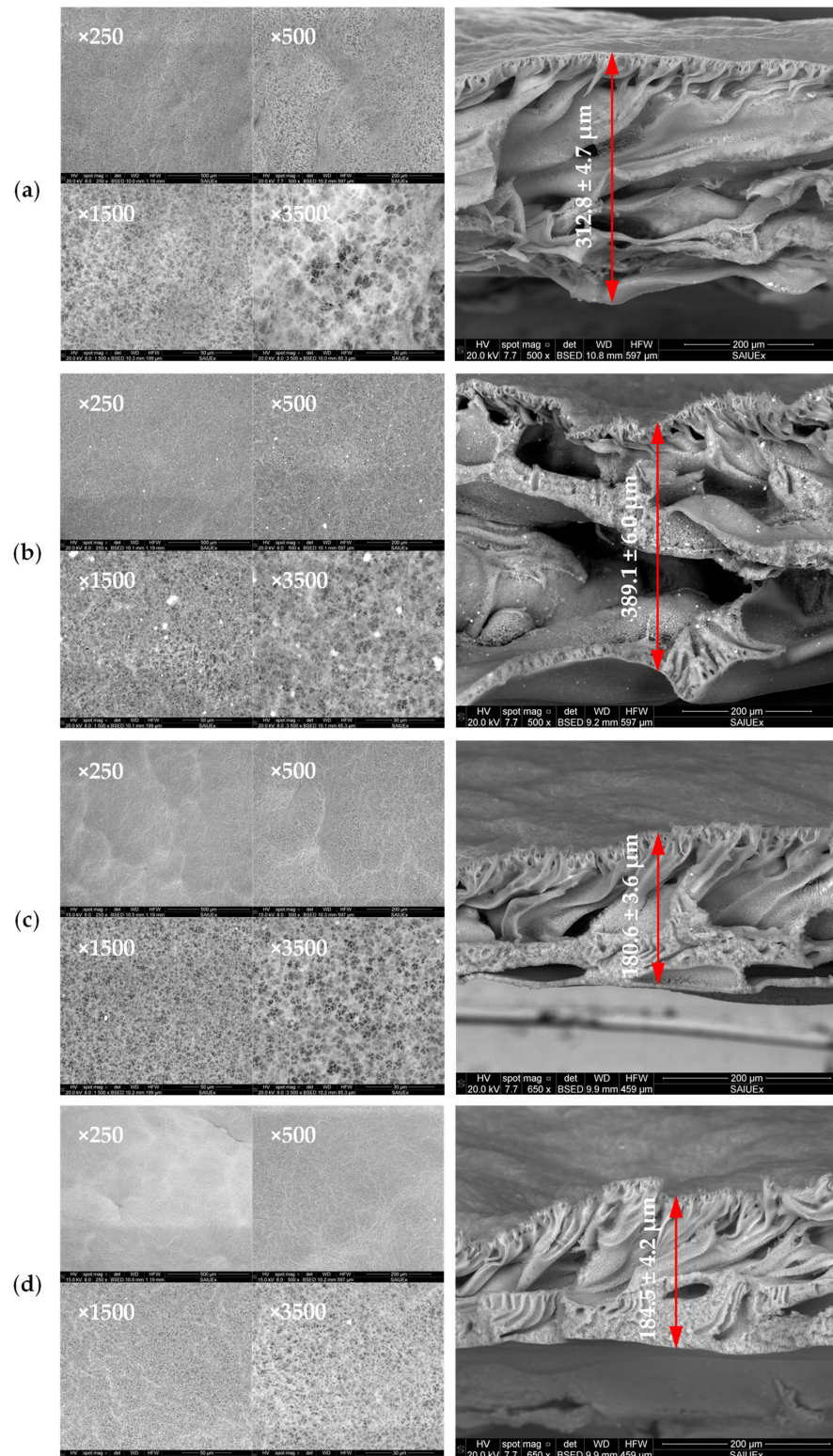


**Figure 3.** SEM images of membranes (a) PVDF, (b) PVDF-P25-1, (c) PVDF-P25-5, and (d) PVDF-P25-8.

Figure 4 displays SEM-EDX images of the PVDF and PVDF/TiO<sub>2</sub> samples. From them, the elemental composition was calculated as shown in Table 2. It can be seen that the PVDF sample had a minor content of oxygen, likely due to the presence of a small amount of residual PVP in the material. As seen in Figure 4, the TiO<sub>2</sub> was well distributed in the PVDF/TiO<sub>2</sub> membranes, although an accumulation of surface Ti in some areas of the PVDF-P25-1 sample was observed as a result of the deposition of TiO<sub>2</sub> agglomerates. Considering the titanium concentrations determined via EDX (Table 2), the estimated TiO<sub>2</sub> concentration would be 2.42, 11.88, and 15.25 wt.% for PVDF-P25-1, PVDF-P25-5, and PVDF-P25-8, respectively.

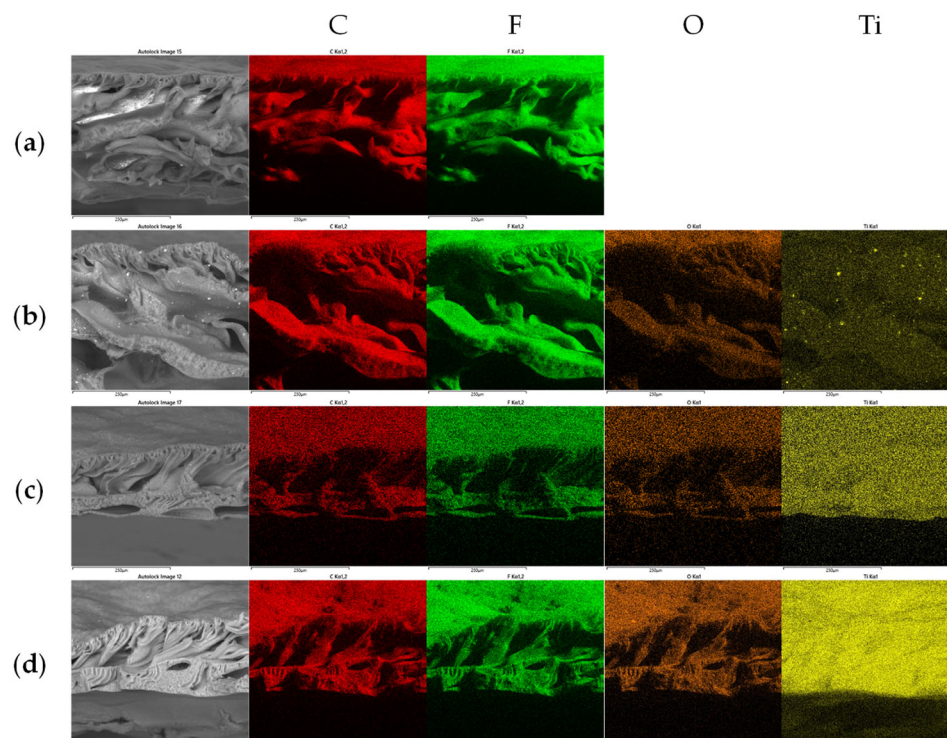


**Figure 4.** SEM-EDX images of membranes (a) PVDF, (b) PVDF-P25-1, (c) PVDF-P25-5, and (d) PVDF-P25-8.

**Table 2.** Elemental composition (estimated results) of the synthesized membranes as obtained from EDX analysis.

Membrane	Elemental Composition (wt.%)			
	C	O	F	Ti
PVDF	54.27 ± 0.06	1.14 ± 0.13	44.59 ± 0.09	-
PVDF-P25-1	50.56 ± 0.27	3.87 ± 0.47	44.13 ± 0.28	1.45 ± 0.03
PVDF-P25-5	42.50 ± 0.15	10.70 ± 0.04	39.67 ± 0.03	7.12 ± 0.15
PVDF-P25-8	40.84 ± 0.59	15.84 ± 0.39	34.19 ± 1.17	9.14 ± 0.22

Figure 5 shows the Fourier transform infrared spectrometer (FTIR) data for the air-dried membranes, including the pristine PVDF membrane and PVDF/TiO<sub>2</sub> membranes both before and after their use in the photocatalytic filtration runs. A group of characteristic peaks confirmed the presence of the PVDF polymer in their  $\alpha$  and  $\beta$  crystalline forms, which is in agreement with other studies from the literature [40,41]. In brief, a peak visible at 762 cm<sup>-1</sup>, which may be the result of CH<sub>2</sub> in-plane bending or scissoring [42], is characteristic only of the  $\alpha$  phase [43]. Likewise, a peak of 1276 cm<sup>-1</sup> was reported to be present only in the  $\beta$  phase [41]. Specific peaks for the  $\gamma$  phase were not detected. Some other peaks present in the spectra of all the samples are attributed to different

modes of vibration of  $\text{CH}_2$ ,  $\text{CF}_2$ , and C-C groups in PVDF [41–44]. Spectra also display an additional peak at  $1663\text{ cm}^{-1}$ , which may be attributed to C=O groups in residual PVP [45]. Overlapping peaks in the  $500\text{--}800\text{ cm}^{-1}$  range in PVDF/ $\text{TiO}_2$  samples are characteristics of Ti-O vibrations [46–48].

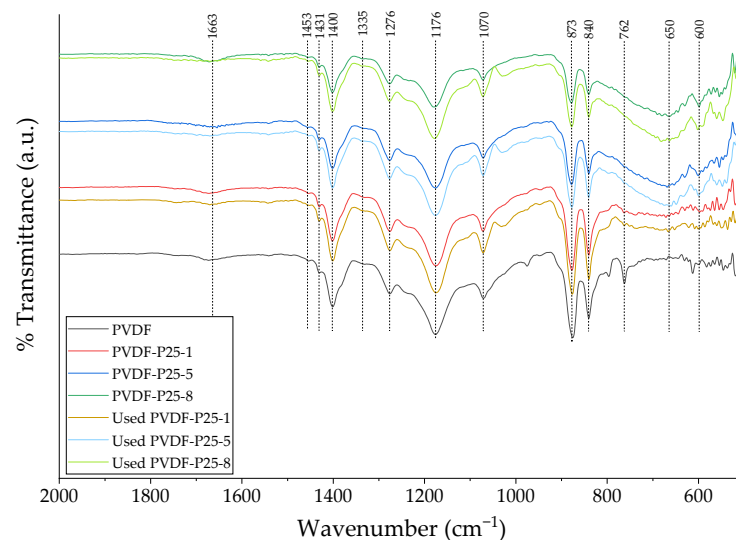


**Figure 5.** FTIR spectra of fresh membranes and PVDF/ $\text{TiO}_2$  membranes after their use in long-term photocatalytic filtration runs.

Regarding membrane stability, no apparent spectral changes were observed upon long-term use of the photocatalytic membranes in agreement with other studies that reported that PVDF/ $\text{TiO}_2$  membranes exhibit high chemical stability and durability [22,32].

The surface components and chemical states of the synthesized membranes were evaluated using X-ray photoelectron spectroscopy (XPS). Figure 6 collects the survey spectra of the four synthesized membranes. High-resolution spectra of the regions C1s and Ti2p are also shown for the PVDF-P25-5 sample as an example. In Figure 6a, all the samples display peaks in the regions C1s and F1s, as expected for PVDF-based materials. In the region C1s, all the samples exhibit peaks at 284.6 eV, 287.0 eV, and 289.2 eV (see Figure 6b), attributed to C-C, H-C-F, and  $\text{CF}_2$  bondings, respectively [49]. Organic and semi-ionic fluorides were detected in the F1s region showing peaks at 687.4 eV and 684.7 eV, respectively [49,50]. As shown in Figure 5, the region Ti2p revealed two different peaks at 464.1 eV (attributed to the  $\text{Ti}^{4+} 2p_{1/2}$ ) and at 458.6 eV (associated with the  $\text{Ti}^{4+} 2p_{3/2}$ ) [29,51]. Other peaks were found in the region O1s, though their assignment was not straightforward as some aluminum and silicon contamination might occur during the manipulation of the membranes. Typically, oxygen-related peaks at 531.5 eV and 529.8 eV are associated to OH groups adsorbed onto the membrane surface and Ti-O bonds in the membrane structure, respectively [29]. From the Ti2p peaks, the surface  $\text{TiO}_2$  composition of the samples could be estimated to be <0.1%, 0.8%, and 0.7% in PVDF-P25-1, PVDF-P25-5, and PVDF-P25-8, respectively. These low values suggest that almost all the  $\text{TiO}_2$  was embedded within the polymeric material with a minor presence on the outer surface. These results are consistent with the measured WCA, as this parameter did not decrease when the  $\text{TiO}_2$  P25 nanoparticles were inserted into the PVDF membrane.



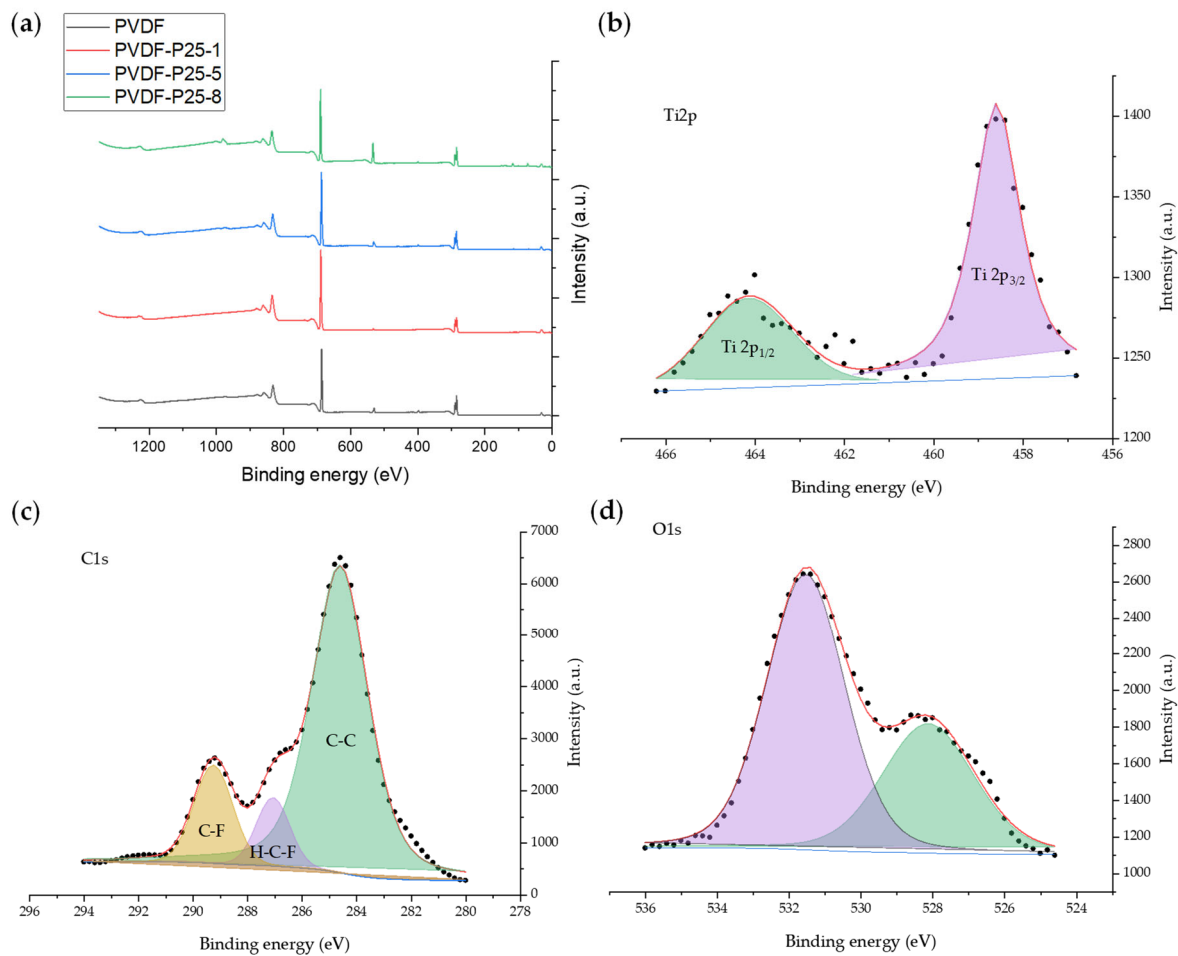


**Figure 6.** XPS (a) survey spectrum of membranes and high-resolution spectra of PVDF-P25-5 membrane for (b) Ti2p, (c) C1s, and (d) O1s regions.

The thermal behavior of the PVDF/TiO<sub>2</sub> membranes was studied via thermogravimetric analysis (TGA and DTG) as shown in Figure 7. The samples PVDF-P25-1 and PVDF-P25-5 started to decompose at 355 °C, while the membranes PVDF-P25-8 and PVDF remained stable up to 374 °C and 450 °C, respectively. A high thermal stability of PVDF has been reported in the literature [52]. The results suggest that the presence of TiO<sub>2</sub> P25 in the samples catalyzes the thermal oxidation reaction, lowering the decomposition temperature.

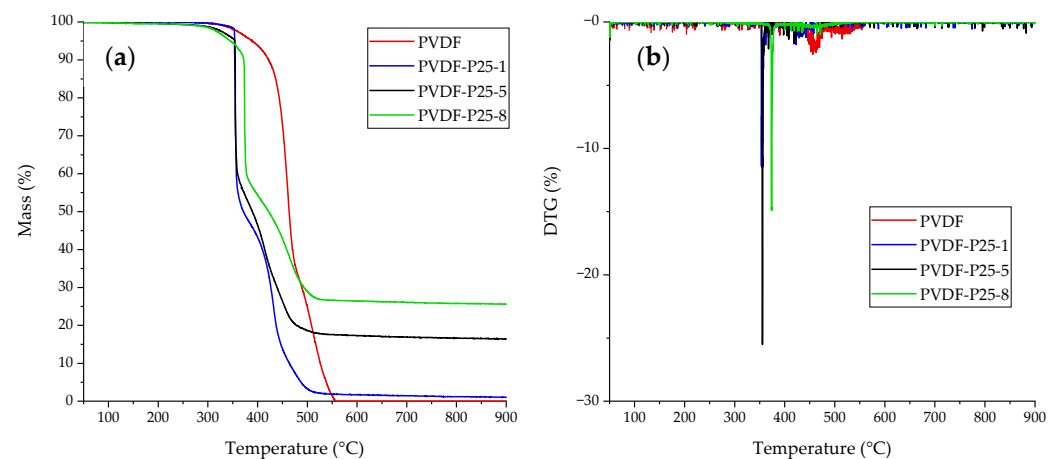


**Figure 7.** (a) TGA and (b) DTG analysis results.



From the ashes collected at the end of the thermal treatments, the  $\text{TiO}_2$  composition in the bulk membranes was estimated to be 1.83 wt.% for PVDF-P25-1, 17.6 wt.% for PVDF-P25-5, and 26.6 wt.% for PVDF-P25-8. These results are different from those obtained via SEM-EDX. At this point, it should be recalled that an EDX analysis gives semi-quantitative information. Therefore, the  $\text{TiO}_2$  composition as obtained from the ash analysis can be considered more accurate.

Figure 8a shows the diffuse reflectance spectra (DRS) of the PVDF-P25 samples together with those of the PVDF and pure  $\text{TiO}_2$  P25. As expected, the sample PVDF did not absorb UV-vis radiation, while the light absorption of the  $\text{TiO}_2$ -P25 and PVDF-P25 samples was limited to the wavelength below 400 nm. This means that the photocatalytic membranes prepared in this work are not visible-light photoresponsive materials. To achieve that goal,  $\text{TiO}_2$ -based heterostructures (e.g.,  $\text{TiO}_2$ -Ag and  $\text{TiO}_2$ -graphene oxide) could be used instead of bare  $\text{TiO}_2$  [53,54]. The Tauc plot method using the Kubelka–Munk function was applied to calculate the band-gap energy of  $\text{TiO}_2$ -P25 and PVDF-P25 samples [55] resulting in similar values for all the samples (Figure 8b). Accordingly, a photocatalytic activation energy of about 3.2 eV (i.e., radiation below 385 nm) was obtained regardless of the  $\text{TiO}_2$  concentration in the membrane. This result agrees with the standard band gap of  $\text{TiO}_2$  P25 accepted by other authors [9]. As mentioned before, this limits the light activation of the catalyst to the UV spectrum. Using visible-responsive materials in the photocatalytic membrane could lower the band-gap energy. Thus, band-gap energies of 2.7 eV, 2.29 eV, and 2.59 eV have been reported for PVDF membranes loaded with  $\text{g-C}_3\text{N}_4$ ,  $\text{TiO}_2$ -Ag heterostructures, and  $\text{TiO}_2$ -graphene oxide, respectively [27,53,54].

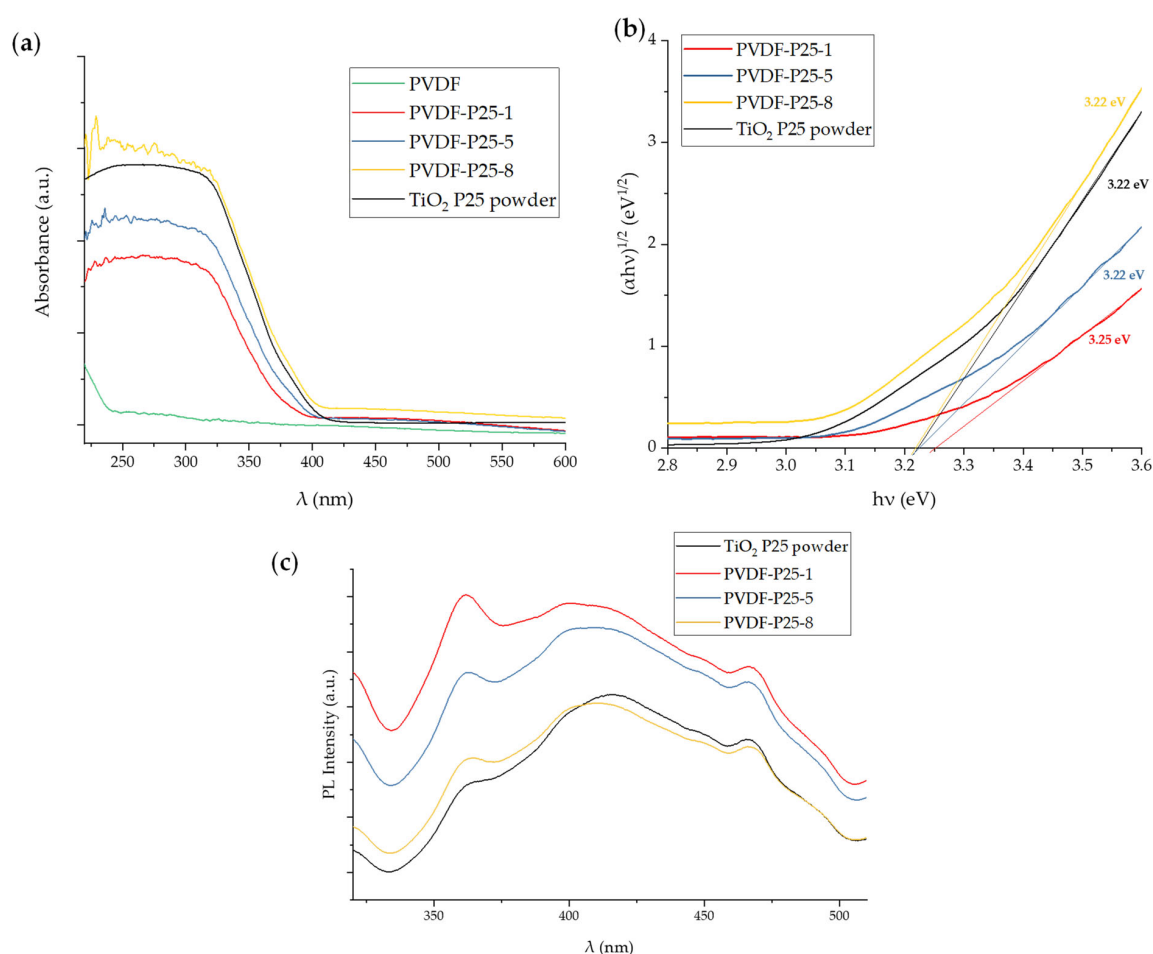


**Figure 8.** (a) UV-Vis spectra, (b) Tauc plots for band-gap calculation, and (c) photoluminescence spectra (excitation wavelength 280 nm) of photocatalytic membranes and  $\text{TiO}_2$  P25 powder.

Photoluminescence (PL) spectroscopy is useful to investigate electron–hole recombination mechanisms in semiconductor materials. Generally, two PL processes can be distinguished upon excitation of a semiconductor with the light energy higher than the band-gap energy. On one hand, there is the band–band PL process due to direct transitions of excited electrons from the conduction band to the valence band top, releasing energy radiation of a wavelength equal or lower than that corresponding to the band-gap energy. On the other hand, there is the excitonic PL process, in which excited electrons go first, through a non-radiative process, from the conduction band to different surface states (i.e., sub-bands) and fall to the valence band top, resulting in a release of energy as radiation of a wavelength higher than the band gap. While the band–band PL process is directly related to the electron–hole recombination, the excitonic PL process arises mainly from surface oxygen vacancies and defects in the semiconductor material [56].

Figure 8c displays the PL spectra of the TiO<sub>2</sub> P25 powder and PVDF-P25 membranes. A broad PL band centered at about 365 nm can be seen in all the materials. According to the discussion above, it can be associated with electron–hole recombination (i.e., the band–band PL process), while other peaks at energies lower than the band-gap energy (i.e.,  $\lambda > 387$  nm) are excitonic PL bands that could arise from TiO<sub>2</sub> surface states [56]. The PL intensity at 365 nm of the PVDF-P25 samples higher than that of TiO<sub>2</sub> P25 suggests that the entrapment of TiO<sub>2</sub> P25 particles in the membrane accelerated the direct electron–hole recombination, which does not favor the photocatalytic activity. Nevertheless, increasing the TiO<sub>2</sub> loading in the PVDF membrane led to a decreased PL intensity and, therefore, an enhanced charge separation.

## 2.2. Ultrapure Water Filtration Experiments

The ultrapure water (UP) permeate flux ( $J_w$ ) was first determined by filtrating the UP (no MPs added) through the membranes for at least 4 h. For this purpose, a 1 mL·min<sup>−1</sup> flow rate was applied to generate the required transmembrane pressure. Table 3 shows the values of the  $J_w$ , both in the absence and presence of radiation. In general, a negligible effect of the radiation was observed for all the membranes. Also, in line with other studies [32,37,38], the UP permeate flux was improved by increasing the TiO<sub>2</sub> dose from PVDF-P25-1 to PVDF-P25-8. Such an enhancement may be explained by the different thicknesses of the membranes (see Figure 3). Thus, membrane PVDF-P25-1 presented the lowest value of the  $J_w$  in agreement with its largest thickness.

**Table 3.**  $J_w$  measurements for produced membranes.

Membrane	$J_w$ (L·m <sup>−2</sup> ·h <sup>−1</sup> )	
	LED Off	LED On
PVDF	240.8	238.4
PVDF-P25-1	210.2	204.8
PVDF-P25-5	256.0	258.3
PVDF-P25-8	292.6	286.2

Filtration experiments were also conducted with a solution of MTP and VEN (initial concentration of 250 µg·L<sup>−1</sup>) in UP. Each run consisted of two stages. Firstly, a dark stage of 3 h in the absence of radiation (LED off) to allow for MPs to be adsorbed on the membrane to an extent close to equilibrium. Then, a radiation stage of 24 h (LED on) to allow for the photocatalytic removal of MPs. The concentration of MPs and the permeate flux ( $J_v$ ) were measured over time. A steady-state permeate flux ( $J_{vss}$ ) was observed in all the experiments. To compare the performance of the different membranes, a mass removal rate parameter ( $MRR$ , mg·m<sup>−2</sup>·h<sup>−1</sup>) was calculated according to Equation (1):

$$MRR_i = J_{vss} \cdot (C_{feed\ i} - C_{ss\ i}) \quad (1)$$

being  $i$  the MP analyzed,  $C_{feed\ i}$  the initial concentration of the MP in the feed stream, and  $C_{ss\ i}$  the average concentration of the MP at steady state.

Figure 9 shows the normalized concentration of the MPs (i.e., MTP and VEN) and the permeate flux during the continuous membrane filtration experiments. It can be seen that the adsorption equilibrium of MTP was practically achieved in the three-hour dark stage, measuring a concentration at  $t = 0$  (when the LED was turned on) almost equal to that of the feed stream. However, the maximum concentration of VEN was not achieved after the dark stage, suggesting a stronger interaction of this compound with the membrane surface. This agrees well with the fact that the  $\log K_{ow}$  of VEN has been reported to be higher than that of MTP [57] (see Table 4). Accordingly, VEN is more hydrophobic than MTP, which suggests stronger non-polar interactions with a relatively hydrophobic membrane. This effect was more noticeable in the filtration experiment with the pristine PVDF membrane, where the VEN equilibrium concentration was achieved after more than 24 h. Furthermore, small variations in the adsorption of the MPs were detected among membranes with different doses of  $TiO_2$  P25. In general, the higher the  $TiO_2$  P25 concentration in the membrane, the lower the amounts of MPs adsorbed. The reason for this is probably the hydrophilic character of  $TiO_2$  P25 and the reduction in the adsorption capacity of the membranes due to the internal presence of  $TiO_2$  P25. In line with this, the adsorption of VEN and MTP on powdered  $TiO_2$  P25 has been reported to be negligible [58,59].

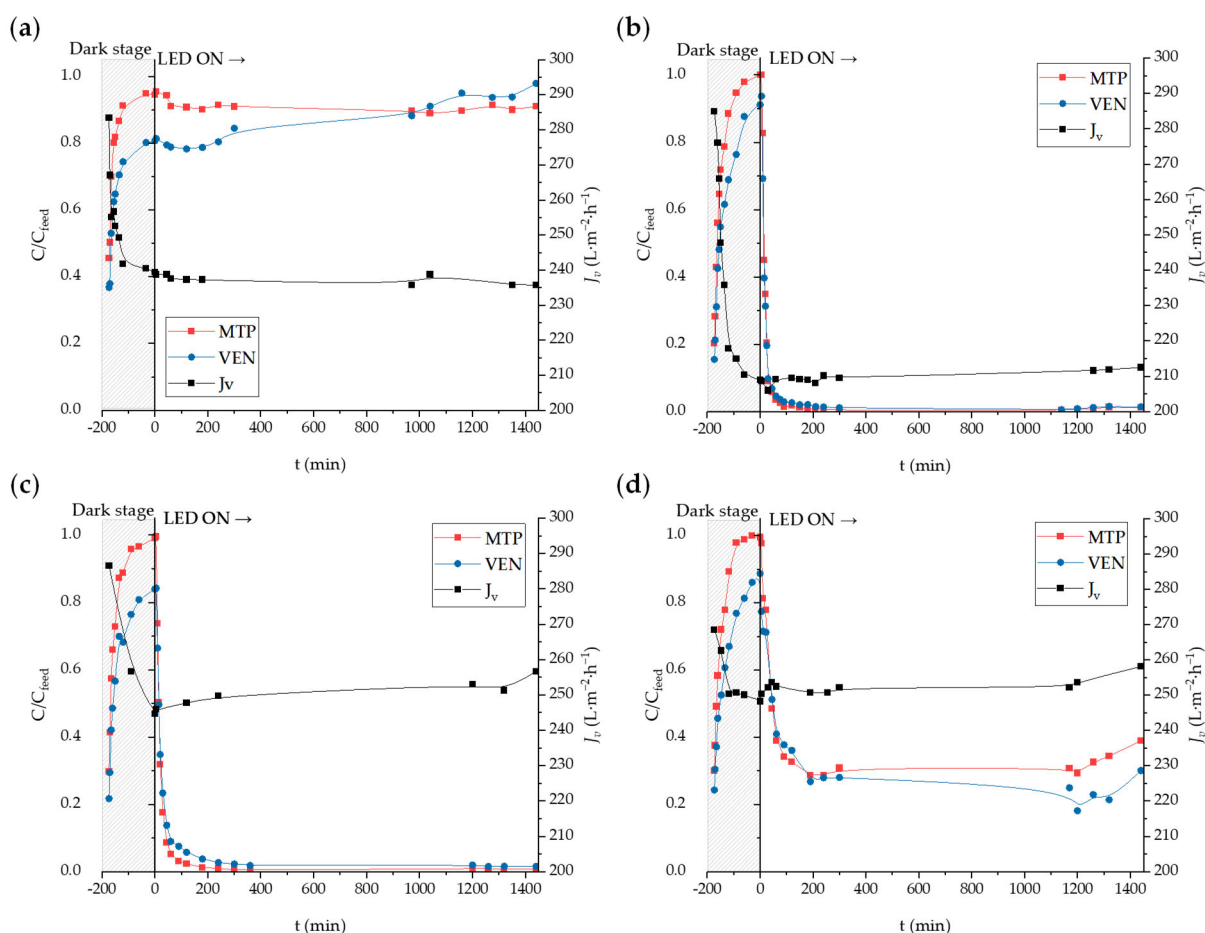


**Figure 9.** MPs elimination in UP experiments using (a) pristine PVDF, (b) PVDF-P25-1, (c) PVDF-P25-5, and (d) PVDF-P25-8 membranes. Shaded areas indicate that the LED was off.

**Table 4.** Physicochemical properties of the MPs used in this study.

MP	Molecular Formula	Molecular Weight (g·mol <sup>−1</sup> )	pK <sub>a</sub>	log K <sub>ow</sub>	Molar Volume (cm <sup>3</sup> )
Venlafaxine (VEN)	C <sub>17</sub> H <sub>27</sub> NO <sub>2</sub>	277.40	9.50	3.20	261.6 ± 3.0
Metoprolol (MTP)	C <sub>15</sub> H <sub>25</sub> NO <sub>3</sub>	267.36	9.56	1.88	258.7 ± 3.0

As it is apparent in Figure 9b–d, the concentration of MPs decreased dramatically just after turning on the UV-LED irradiation. However, the concentration of MPs remained fairly constant when the pristine PVDF membrane was irradiated (Figure 9a), indicating the absence of photolysis of the selected MPs at the LED emission wavelength (i.e., 375 nm). The steady-state removal efficiencies achieved with PVDF-P25-1 and PVDF-P25-5 were close to each other and very high, achieving up to 99% elimination for both MPs. However, it is important to notice that the permeate flux was higher using PVDF-P25-5, so the MRR was also higher (see Table 5). Even though some MP elimination was observed with PVDF-P25-8, the removal rate was significantly lower than those obtained with the other PVDF/TiO<sub>2</sub> membranes, reaching elimination percentages of around 72% for both MPs at the steady state (Figure 9d). Nonetheless, it is worth noting that as the  $J_{vss}$  was higher than in the case of PVDF-P25-1, the MRR results were similar for PVDF-P25-1 and PVDF-P25-8 (see Table 5). These results in UP allow us to state that, among the tested membranes, PVDF-P25-5 appeared to be the most efficient in terms of the MRR.

**Table 5.** Permeate flux and MRR results in UP filtration experiments.

Membrane	$J_{vss}$ (L·m <sup>−2</sup> ·h <sup>−1</sup> )	$J_{vss}/J_w$	MRR (mg·m <sup>−2</sup> ·h <sup>−1</sup> )	
			MTP	VEN
PVDF	236.6	0.988	–	–
PVDF-P25-1	211.1	1.017	48.3	45.0
PVDF-P25-5	253.7	0.986	66.3	65.3
PVDF-P25-8	254.7	0.880	45.9	49.0

The MRR results obtained in this work cannot be easily compared with others from the literature due to differences in the permeate flux. Thus, MRR values as low as 19.9 and 20.6 mg·m<sup>−2</sup>·h<sup>−1</sup> are reported for the removal of MTP and VEN, respectively, using PVDF/g-C<sub>3</sub>N<sub>4</sub> membranes activated with visible light and operating with a permeate flux of 89.5 L·m<sup>−2</sup>·h<sup>−1</sup>. In contrast, Dekkouche et al. observed a faster removal of VEN using a TiO<sub>2</sub>-coated PVDF membrane (a permeate flux of about 1200 L·m<sup>−2</sup>·h<sup>−1</sup>) [32].

The removal mechanism of the MPs via water filtration through the PVDF/TiO<sub>2</sub> membranes in our tests comprised two steps in series: first, the MPs were adsorbed onto the membrane in the absence of radiation; then, the LED lamp was switched on and, in addition to the adsorption of MPs, photocatalytic removal took place. As TiO<sub>2</sub> P25 was the photoactive species, the illumination of the PVDF/TiO<sub>2</sub> membrane allowed for the embedded TiO<sub>2</sub> particles to absorb radiation of enough energy to produce photo-excited electron–hole pairs. Then, photo-excited charges were transported to the TiO<sub>2</sub> surface, where electrons (e<sup>−</sup>) react with dissolved oxygen to produce superoxide radical species (•O<sub>2</sub><sup>−</sup>) while holes (h<sup>+</sup>) react with H<sub>2</sub>O/OH<sup>−</sup> to yield hydroxyl radical species (HO•). In turn, superoxide radicals participate in a free-radical chain mechanism leading to the generation of HO• [60]. Therefore, different oxidizing species (i.e., h<sup>+</sup>, •O<sub>2</sub><sup>−</sup>, and HO•) could be responsible for the degradation of VEN and MTP (both adsorbed onto the membrane and in the water bulk). However, it is thought that HO• is the main reactive species because its formation is favored and the reaction rate with the MPs is higher than those of h<sup>+</sup> and •O<sub>2</sub><sup>−</sup> [61]. From Figure 9, it can be seen that, regardless of the PVDF/TiO<sub>2</sub>



membrane used, the removal rates of MTP and VEN were close to each other. The similar reactivity of these MPs with  $\text{HO}^\bullet$  (rate constants of  $6.92 \times 10^9$  and  $8.0 \times 10^9 \text{ L}\cdot\text{mol}^{-1}\cdot\text{s}^{-1}$  for VEN and MTP, respectively [62,63]) explains these results.

A flux decline may be produced mainly via concentration polarization, gel or cake formation, adsorption, and pore blocking [64]. In brief,  $J_v$  is normally reduced initially due to either gel or cake formation or pore blocking [65] and can also be affected by the concentration polarization effect, produced by the accumulation of adsorbed materials within the boundary region of the membrane [66].

During the UP experiments carried out in this work, the permeate flux resulted close to  $1 \text{ mL}\cdot\text{min}^{-1}$  in all cases at the beginning of each test, but soon it dropped and reached a steady-state value ( $J_{vss}$ ). The data of the  $J_{vss}$  and the ratio  $J_{vss}/J_w$  can be found in Table 5.  $J_{vss}/J_w$  is the ratio between the steady-state permeate flux for the solution containing the MP and that corresponding to the filtration of UP without an MP. In this regard, the adsorption of contaminants onto the membranes appeared to be the main cause of fouling, only evident when using the PVDF-P25-8 membrane ( $J_{vss}/J_w$  of 0.88), while the other membranes resulted in low membrane fouling ( $J_{vss}/J_w$  close to 1), probably because of the low pollutant concentration used.

After illuminating the photocatalytic membranes, the permeate flux seemed to slightly increase, possibly because of the self-cleaning effect of the membrane (i.e., elimination of adsorbed substances). However, this enhancement was not great as in most cases  $J_v$  was almost equal to  $J_w$ .

It is worth noting that the PVDF-P25-5 and PVDF-P25-8 membranes resulted in being physically damaged after their long-term use (see Figure 10) both in the presence and absence of radiation (dark or illuminated stage). A reduction in the tensile strength of this type of material has been reported while increasing the  $\text{TiO}_2$  composition [35], suggesting that these membranes might not cope well with the experimental setup and flow conditions (see Section 3 of this article) applied in this work. To avoid this membrane mechanical failure, the applied water flow rate could be reduced and/or a mechanical support for the membrane could be installed in the experimental device.



**Figure 10.** Picture of a membrane with physical damage after UP filtration.

### 2.3. Secondary Effluent Filtration Experiments

After the UP filtration experiments were performed, a secondary effluent (SE) was used to investigate the effect of the SE matrix on the photocatalytic process. For comparison purposes, the membrane PVDF-P25-1 was selected as it showed good performance as well as better mechanical strength than the others. Firstly, the SE was prefiltered with a fiberglass filter to reduce the suspended solids and avoid cake layer formation on the membrane surface. In order to test the influence of the carbonate/bicarbonate anions present in the SE, a modified SE (i.e., SE2) was also prepared. Figure 11 shows the results of the photocatalytic filtration experiments with SE1 (raw SE) and SE2 (partial removal of carbonate/bicarbonate from SE).

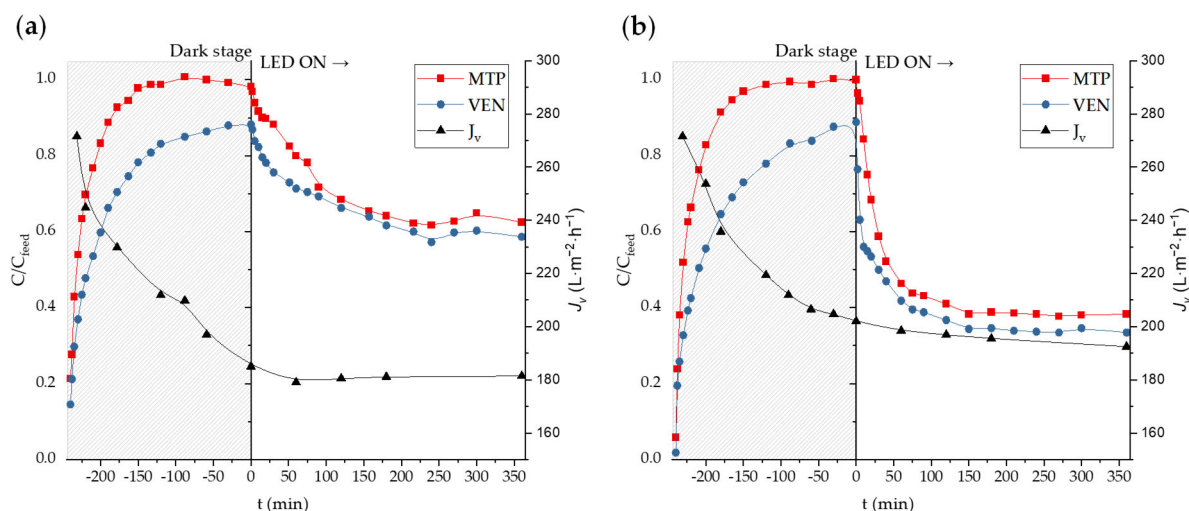


**Figure 11.** MPs elimination experiments using PVDF-P25-1 membrane in (a) SE1 and (b) SE2. Shaded areas indicate that the LED was off.

In contrast to the UP experiments, the adsorption stage was carried out for 4 h instead of 3. The reason for this was to potentiate the maximum adsorption saturation of the membrane before starting the photocatalytic process. The MTP reached the saturation level within 2 h of filtration, whereas the VEN did not reach adsorption equilibrium, which is similar to that observed in the experiments with UP. It should be pointed out that the MP concentration (either MTP or VEN) in the permeate at 3 h of the dark stage was higher than that achieved using UP, indicating that the organic and inorganic matter present in the SE negatively affected the adsorption capacity of both MPs.

After the first stage of the experiment, the LED was turned on to start the photocatalytic oxidation phase, which lasted 6 h as shown in Figure 11. As expected, the removal rate of both the VEN and MTP was highly affected when using an SE as a water matrix. The elimination percentage in SE1 was reduced from 99% in UP to 35 and 38% for MTP and VEN, respectively. Table 6 summarizes the *MRR* and other filtration parameters obtained from the UP, SE1, and SE2 experiments. It can be seen that when treating SE1, the *MRR* fell more than 60% (with regard to the UP run) for both MPs, confirming that components of SE1 had a negative impact on the efficiency of the photocatalytic process to remove the MPs.

**Table 6.** Permeate flux and *MRR* results in UP and SE filtration experiments with PVDF-P25-1.

Matrix	$J_{vss}$ (L·m <sup>-2</sup> ·h <sup>-1</sup> )	$J_{vss}/J_w$	<i>MRR</i> (mg·m <sup>-2</sup> ·h <sup>-1</sup> )	
			MTP	VEN
UP	211.1	1.017	48.3	45.0
SE1	181.0	0.872	17.3	18.5
SE2	195.8	0.944	30.7	32.2

Carbonate/bicarbonate anions have been reported to be hydroxyl radical scavengers naturally present in secondary effluents from WWTPs [67,68]. Accordingly, the elimination percentages and *MRR* of the MPs were higher in the SE2 experiment than in the SE1 run, reaching removals of 61% and 66% for the MTP and VEN, respectively. In addition, the *MRR* values were significantly higher than those obtained with SE1, demonstrating that the carbonate/bicarbonate content constitutes a major scavenging agent in the photocatalytic process.

The total organic carbon (TOC) was measured at the beginning and at the end of each experiment, resulting in a negligible variation of this parameter. Considering that SE organic matter was the major TOC contribution due to the low concentration of the spiked

MPs, it is possible to state that this process was not able to remove the organic matter naturally present in the SE to a large extent.

Figure 11 also shows the time evolution of the  $J_v$  in the SE1 and SE2 experiments. A similar flux decline profile was measured compared to the UP experiments. However, the values of  $J_{vss}$  (see Table 6) were lower with both SE1 and SE2 than with UP, showing that the effect of fouling was likely produced by the suspended solids present in the SE as well as DOC. Despite the observed decrease in the  $J_v$  with time, it should be noticed that the permeate remained above 87% of the maximum  $J_w$  value in both cases. The membrane fouling was slightly lower in the experiment performed with SE2. During the carbonate/bicarbonate elimination process, some suspended solids were also removed, which could be a reason for the lower fouling observed in the experiment with SE2.

### 3. Materials and Methods

#### 3.1. Materials

The pollutants VEN (hydrochloride acid salt, CAS 99300-78-4) and MTP (tartrate salt, CAS 56392-17-7) were purchased from Sigma-Aldrich (Burlington, MA, USA), both of 98% purity. Their physicochemical properties are summarized in Table 4, with all values obtained from PubChem (Bethesda, MD, USA) except the molar volumes, which were estimated using the software ChemsSketch v.2023.1.2, from ACD/Labs (Toronto, ON, Canada). The PVDF pellets (average molecular weight 275,000, CAS 24937-79-9), PVP (average molecular weight 40,000, CAS 9003-39-8), and 1-methyl-2-pyrrolidone (NMP, CAS 872-50-4, >99% purity) were obtained from Sigma-Aldrich. The AEROXIDE® titanium dioxide P25 (CAS 13463-67-7) was obtained from Evonik Industries AG (Essen, Germany). The HPLC-grade acetonitrile (CAS 75-05-08) was acquired from Honeywell Riedel-de Haën (Seelze, Germany), orthophosphoric acid (CAS 7664-38-2, 85%) was obtained from Panreac (Castellar del Vallès, Spain), and UP was generated using a Milli-Q system from Millipore (Burlington, MA, USA).

The SE from a municipal WWTP located in the region of Extremadura (Southwest Spain) was used as a matrix to test the performance of the photocatalytic membrane treatment. This effluent was prefiltered using a glass microfiber filter (1.2 µm pore size) from VWR (USA) to eliminate the solid particles from the matrix and then stored in a refrigerator at 5 °C until further use within 5 days. In addition, to investigate the influence of carbonate/bicarbonate ions, the SE was modified to adjust its total inorganic carbon (TIC) to about 10 mg L<sup>-1</sup>. The main characteristics of both the unmodified SE (SE1) and modified SE (SE2) are shown in Table 7.

**Table 7.** Secondary effluent characterization after prefiltration.

Parameter	SE1	SE2
pH	7.67	7.37
Electric conductivity (µS·cm <sup>-1</sup> )	1171	1136
Turbidity (NTU)	2.31	2.16
COD (mg·L <sup>-1</sup> )	21	24
TOC (mg·L <sup>-1</sup> )	6.05	6.29
TIC (mg·L <sup>-1</sup> )	89.7	9.55
Absorbance (254 nm)	0.119	0.123
Total N (mg·L <sup>-1</sup> )	5.2	5.0
Total P (mg·L <sup>-1</sup> )	0.29	0.28

#### 3.2. Membrane Synthesis and Characterization

The membranes were synthesized according to a method already described in the literature [69]. Briefly, the procedure started by mixing 0.1 g of PVP with the desired amount of TiO<sub>2</sub> P25 (0 for pristine PVDF membrane; 0.1 g PVDF-P25-1; 0.5 g for PVDF-P25-5; and 0.8 g for PVDF-P25-8) in 8.4 mL of NMP. Then, the mixture was sonicated in an ultrasonic bath for 3 h before adding 1.5 g of PVDF pellets. After that, the suspension was stirred at

250 rpm and 40 °C for 48 h. Finally, the resulting suspension was left overnight to allow for the air bubbles to be removed prior to membrane fabrication.

For membrane production, an Elcometer 3580 (Manchester, UK) casting knife was used. The polymeric solution was spread onto a glass flat surface with a thickness of 500  $\mu\text{m}$ . The polymeric liquid layer was later soaked into a coagulation UP bath for a few seconds to carry out a phase inversion process. The membrane sheets were stored in UP until use, when the membranes were cut into 26 mm diameter circles to fit the filtration cell.

The synthesized membranes were characterized using different analytical techniques. The surface hydrophobicity was determined by measuring the UP contact angles using the sessile drop method with an Attension Theta Optical Tensiometer by Biolin Scientific (Gothenburg, Sweden). The optical band gap was determined via DRUV/Vis on a JASCO V 560 (Madrid, Spain) spectrophotometer. The photoluminescence spectra were acquired on a JASCO FP-8300 spectrofluorometer (Madrid, Spain). The functional groups were studied using a JASCO FTIR FT/IR-6800 spectrometer (Madrid, Spain) equipped with an attenuated total reflectance MIRacle™ Single Reflection sampling accessory (ZnSe crystal plate) (from PIKE Technologies, Madison, WI, USA) between 3000 and 500  $\text{cm}^{-1}$ . The nitrogen adsorption–desorption isotherms were produced on a Quantachrome NOVA 4200e (Odelzhausen, Germany) apparatus. A NETZSCH STA 409 PC (Selb, Germany) thermobalance was used to study the pyrolytic degradation of the membranes at a heating rate of 5  $^{\circ}\text{C}\cdot\text{min}^{-1}$ . The morphology and elemental composition of the membranes were determined by using an SEM-EDX device, model FEI QUANTA 3D FEG (Hillsboro, OR, USA). In addition, the surface composition was analyzed using the XPS equipment SPECS FlexPS-ARPES-E (Berlin, Germany).

### 3.3. Experimental Procedure

The experimental setup used to evaluate the capability of the synthesized membranes to remove specific MPs (i.e., VEN and MTP) in water is illustrated in Figure 12 [27]. The setup included a 10 W LED (peak emission wavelength of 375 nm according to the manufacturer). It was placed next to the membrane module wall, separated 24 mm from the membrane itself. The light emission for characterization purposes was evaluated using an Ocean Optics USB2000+ Fiber Optic Spectrometer (Orlando, FL, USA). The irradiance was measured, giving a value of 4.23  $\text{W}\cdot\text{m}^{-2}$ . In addition, the maximum wavelength of the emitted radiation was measured to be 375 nm.

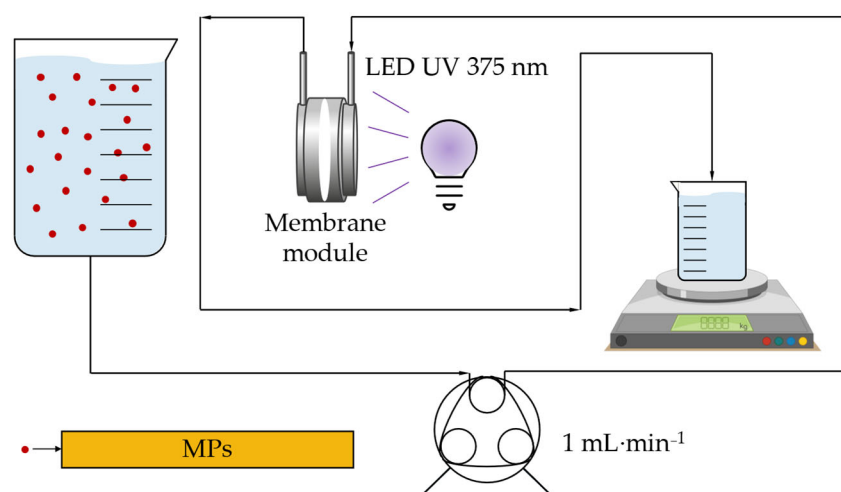


**Figure 12.** Experimental filtration setup scheme.

In brief, a continuous filtration system was set up using a dead-end membrane filtration module capable of fitting 26 mm diameter membranes (actual filtration surface area of 201.06  $\text{mm}^2$ ; illuminated reactor volume of 4.4 mL). Feed water (spiked with 250  $\mu\text{g}\cdot\text{L}^{-1}$  of the MPs) was pumped into the module by using a peristaltic pump (2-channel pump



Ismatec Reglo Analog, flow rate  $1 \text{ mL} \cdot \text{min}^{-1}$ ), which led the fluid to go through the membrane. The tests were conducted at room temperature. The permeate was collected in a beaker placed on an analytical balance to measure the actual permeate flux. Each experiment run consisted of two sequential stages: the first was in the dark (i.e., LED off) to allow for the MPs to adsorb into the membrane until equilibrium was approached; second, the LED was turned on to allow for the photocatalytic process to begin. All these experiments were replicated at least twice.

### 3.4. Analytical Methods

The MP concentration was determined via the Ultra-Performance Liquid Chromatography technique (UPLC), using a Shimadzu (Kioto, Japan) apparatus equipped with a diode-array and fluorescence detector. The column used (Kinetex  $1.7 \mu\text{m}$  XB-C18  $100 \text{ \AA}$   $100 \times 2.1 \text{ mm}$ ) was purchased from Phenomenex (Torrance, California, CA, USA). Buffered UP (0.1% formic acid) and acetonitrile were used as the mobile phase, working in gradient mode at a  $0.25 \text{ mL} \cdot \text{min}^{-1}$  flow rate. Both VEN and MTP were detected and quantified via fluorescence, using an excitation wavelength of 230 nm and an emission wavelength of 300 nm.

In the SE experiments, the TOC and TIC were evaluated on an AnalytikJena TOC-multi N-C 3100 (Jena, Germany), using the NPOC method.

Other analytical procedures for SE characterization were conducted according to Standard Methods [70] using Hanna Instruments (Smithfield, RI, USA) test kits.

## 4. Conclusions

In this work, the  $\text{TiO}_2$  P25 particles were easily embedded into a polymeric structure by a mixed-matrix method, giving rise to PVDF/ $\text{TiO}_2$  photocatalytic membranes. From the characterization analyses, it was proven that the  $\text{TiO}_2$  P25 particles were well distributed in the PVDF matrix rather than remaining on its outer surface. This helped prevent leaching during the filtration tests. Also, the presence of  $\text{TiO}_2$  P25 led to high membrane permeability and anti-fouling behavior. The chemical stability of the prepared PVDF/ $\text{TiO}_2$  membranes was demonstrated via an FTIR analysis of the samples after long-term use in the filtration experiments. However, while the membranes with up to 17.6 wt.% of  $\text{TiO}_2$  P25 showed good mechanical resistance, the membranes with higher  $\text{TiO}_2$  content were at risk of mechanical failure in the experimental setup used in this study for the continuous-mode filtration runs.

The VEN and MTP were removed by up to 99% from the UP aqueous solution using the membranes PVDF-P25-1 and PVDF-P25-5. However, these removal percentages decreased drastically in the SE due to the effect of naturally present substances in such a complex matrix. The high concentration of carbonate/bicarbonate ions in the SE was identified as a major cause of inhibition of the photocatalytic oxidation. Thus, after the partial removal of these species from the SE, the photocatalytic performance was clearly improved.

**Author Contributions:** Conceptualization, J.C.A., A.M.T.S., J.L.A. and P.M.Á.; methodology, J.C.A. and M.P.; validation, J.C.A. and M.P.; formal analysis, J.C.A. and M.P.; investigation, J.C.A., M.P., J.L.A. and P.M.Á.; resources, A.M.T.S., J.L.F., J.L.A. and P.M.Á.; writing—original draft preparation, J.C.A.; writing—review and editing, J.C.A., M.P., A.M.T.S., J.L.A. and P.M.Á.; visualization, J.C.A.; supervision, A.M.T.S., J.L.A. and P.M.Á.; project administration, A.M.T.S., J.L.A. and P.M.Á.; funding acquisition, A.M.T.S., J.L.F., J.L.A. and P.M.Á. All authors have read and agreed to the published version of the manuscript.

**Funding:** This research was mainly funded by the Spanish Ministerio de Ciencia e Innovación and Agencia Estatal de Investigación (MCIN/AEI/10.13039/501100011033), grant number PID2020-113389RB-I00. This work was also supported by Portuguese national funds through FCT/MCTES (PIDDAC): LSRE-LCM, UIDB/50020/2020 (DOI: 10.54499/UIDP/50020/2020) and ALiCE, LA/P/0045/2020 (DOI: 10.54499/LA/P/0045/2020).

**Data Availability Statement:** The release of most of the raw data presented in this study would be facilitated upon request. Some would not be available due to privacy restrictions.

**Acknowledgments:** The authors gratefully acknowledge the services of SAIUEX at the University of Extremadura (Spain), providing some of the membrane characterization techniques. Juan C. Aldana acknowledges his scholarship FPU18/01553 and EST22/00257, funded by MCIN/AEI/10.13039/501100011033 and by “ESF Investing in your future”. Marta Pedrosa acknowledges FCT funding under the 5th Edition Call for Scientific Employment Stimulus—Individual Contract (2022.00192.CEECIND; DOI: 10.54499/2022.00192.CEECIND/CP1733/CT0002).

**Conflicts of Interest:** The authors declare no conflicts of interest.

## References

1. Moratalla, Á.; Correia, S.E.; Lacasa, E.; Murillo, P.; Cañizares, P.; Rodrigo, M.A.; Sáez, C. Facing the Treatment of Polymedicated Effluents Using Gaseous Ozone Electrochemically Generated. *J. Water Process Eng.* **2023**, *55*, 104153. [\[CrossRef\]](#)
2. Arman, N.Z.; Salmiati, S.; Aris, A.; Salim, M.R.; Nazifa, T.H.; Muhamad, M.S.; Marpongahtun, M.; Ben Ayed, L.; Golomazou, E.; Karanis, P.; et al. A Review on Emerging Pollutants in the Water Environment: Existences, Health Effects and Treatment Processes. *Water* **2021**, *13*, 3258. [\[CrossRef\]](#)
3. Tong, X.; Mohapatra, S.; Zhang, J.; Tran, N.H.; You, L.; He, Y.; Gin, K.Y.H. Source, Fate, Transport and Modelling of Selected Emerging Contaminants in the Aquatic Environment: Current Status and Future Perspectives. *Water Res.* **2022**, *217*, 118418. [\[CrossRef\]](#) [\[PubMed\]](#)
4. Bacci, F.; Campo, P. Emerging and Less Commonly Recognized Chemical Contaminants: Organic Micropollutants. In *Encyclopedia of Inland Waters*; Elsevier: Amsterdam, The Netherlands, 2022; Volume 4, pp. 247–259.
5. Lv, J.; Ou, C.; Fu, M.; Xu, Z. Characteristics and Transformation Pathways of Venlafaxine Degradation during Disinfection Processes Using Free Chlorine and Chlorine Dioxide. *Chemosphere* **2021**, *276*, 130147. [\[CrossRef\]](#) [\[PubMed\]](#)
6. Hussain, S.; Ramnarayanan, C.; Roopashree, T.S.; Anwer, M.K.; Sreeharsha, N.; Nair, A.B. Rapid, Precise and Affordable Estimation of Venlafaxine and Its Metabolites in Highly Polluted Effluent Waters: Proof-of-Concept for Methodology. *Molecules* **2020**, *25*, 4793. [\[CrossRef\]](#) [\[PubMed\]](#)
7. Lima, D.L.D.; Silva, C.P.; Otero, M. Dispersive Liquid-Liquid Microextraction for the Quantification of Venlafaxine in Environmental Waters. *J. Env. Manag.* **2018**, *217*, 71–77. [\[CrossRef\]](#) [\[PubMed\]](#)
8. Rutere, C.; Posselt, M.; Ho, A.; Horn, M.A. Biodegradation of Metoprolol in Oxic and Anoxic Hyporheic Zone Sediments: Unexpected Effects on Microbial Communities. *Appl. Microbiol. Biotechnol.* **2021**, *105*, 6103–6115. [\[CrossRef\]](#)
9. Kumari, P.; Bahadur, N.; Dumée, L.F. Photo-Catalytic Membrane Reactors for the Remediation of Persistent Organic Pollutants—A Review. *Sep. Purif. Technol.* **2020**, *230*, 115878. [\[CrossRef\]](#)
10. Qing, W.; Liu, F.; Yao, H.; Sun, S.; Chen, C.; Zhang, W. Functional Catalytic Membrane Development: A Review of Catalyst Coating Techniques. *Adv. Colloid Interface Sci.* **2020**, *282*, 102207. [\[CrossRef\]](#)
11. Pérez-Lucas, G.; El Aatik, A.; Aliste, M.; Navarro, G.; Fenoll, J.; Navarro, S. Removal of Contaminants of Emerging Concern from a Wastewater Effluent by Solar-Driven Heterogeneous Photocatalysis: A Case Study of Pharmaceuticals. *Water Air Soil Pollut.* **2023**, *234*, 1–13. [\[CrossRef\]](#)
12. Jiang, X.; Manawan, M.; Feng, T.; Qian, R.; Zhao, T.; Zhou, G.; Kong, F.; Wang, Q.; Dai, S.; Pan, J.H. Anatase and Rutile in Evonik Aeroxide P25: Heterojunctioned or Individual Nanoparticles? *Catal. Today* **2018**, *300*, 12–17. [\[CrossRef\]](#)
13. Tung, T.X.; Xu, D.; Zhang, Y.; Zhou, Q.; Wu, Z. Removing Humic Acid from Aqueous Solution Titanium Dioxide: A Review. *Pol. J. Environ. Stud.* **2018**, *28*, 529–542. [\[CrossRef\]](#)
14. Mahy, J.G.; Wolfs, C.; Mertes, A.; Vreuls, C.; Drot, S.; Smeets, S.; Dircks, S.; Boergers, A.; Tuerk, J.; Lambert, S.D. Advanced Photocatalytic Oxidation Processes for Micropollutant Elimination from Municipal and Industrial Water. *J. Environ. Manag.* **2019**, *250*, 109561. [\[CrossRef\]](#)
15. Dlamini, M.C.; Maubane-Nkadimeng, M.S.; Moma, J.A. The Use of TiO<sub>2</sub>/Clay Heterostructures in the Photocatalytic Remediation of Water Containing Organic Pollutants: A Review. *J. Environ. Chem. Eng.* **2021**, *9*, 106546. [\[CrossRef\]](#)
16. López, J.; Rey, A.; Viñuelas-Zahinos, E.; Álvarez, P.M. Preparation of a New Green Magnetic Fe<sub>3</sub>O<sub>4</sub>@TiO<sub>2</sub>-P25 Photocatalyst for Solar Advanced Oxidation Processes in Water. *J. Environ. Chem. Eng.* **2023**, *11*, 109999. [\[CrossRef\]](#)
17. Checa, M.; Montes, V.; Rivas, J.; Beltrán, F.J. Checking the Efficiency of a Magnetic Graphene Oxide–Titania Material for Catalytic and Photocatalytic Ozonation Reactions in Water. *Catalysts* **2022**, *12*, 1587. [\[CrossRef\]](#)
18. Zou, D.; Lee, Y.M. Design Strategy of Poly(Vinylidene Fluoride) Membranes for Water Treatment. *Prog. Polym. Sci.* **2022**, *128*, 101535. [\[CrossRef\]](#)
19. Chon, K.; Cho, J.; Shon, H.K. A Pilot-Scale Hybrid Municipal Wastewater Reclamation System Using Combined Coagulation and Disk Filtration, Ultrafiltration, and Reverse Osmosis: Removal of Nutrients and Micropollutants, and Characterization of Membrane Fouling. *Bioresour. Technol.* **2013**, *141*, 109–116. [\[CrossRef\]](#) [\[PubMed\]](#)
20. Li, N.; Lu, X.; He, M.; Duan, X.; Yan, B.; Chen, G.; Wang, S. Catalytic Membrane-Based Oxidation-Filtration Systems for Organic Wastewater Purification: A Review. *J. Hazard. Mater.* **2021**, *414*, 125478. [\[CrossRef\]](#)

21. Gokulakrishnan, S.A.; Arthanareeswaran, G.; László, Z.; Veréb, G.; Kertész, S.; Kweon, J. Recent Development of Photocatalytic Nanomaterials in Mixed Matrix Membrane for Emerging Pollutants and Fouling Control, Membrane Cleaning Process. *Chemosphere* **2021**, *281*, 130891. [\[CrossRef\]](#)
22. Zhang, W.; Zhang, Y.; Fan, R.; Lewis, R. A Facile TiO<sub>2</sub>/PVDF Composite Membrane Synthesis and Their Application in Water Purification. *J. Nanoparticle Res.* **2016**, *18*, 1–10. [\[CrossRef\]](#)
23. Damodar, R.A.; You, S.J.; Chou, H.H. Study the Self Cleaning, Antibacterial and Photocatalytic Properties of TiO<sub>2</sub> Entrapped PVDF Membranes. *J. Hazard. Mater* **2009**, *172*, 1321–1328. [\[CrossRef\]](#)
24. Erusappan, E.; Thiripuranthagan, S.; Radhakrishnan, R.; Durai, M.; Kumaravel, S.; Vembuli, T.; Kaleekkal, N.J. Fabrication of Mesoporous TiO<sub>2</sub>/PVDF Photocatalytic Membranes for Efficient Photocatalytic Degradation of Synthetic Dyes. *J. Environ. Chem. Eng.* **2021**, *9*, 105776. [\[CrossRef\]](#)
25. Li, C.; Yu, H.; Huang, B.; Liu, G.; Guo, Y.; Zhu, H.; Yu, B. Fabrication of Anatase TiO<sub>2</sub>/PVDF Composite Membrane for Oil-in-Water Emulsion Separation and Dye Photocatalytic Degradation. *Membranes* **2023**, *13*, 364. [\[CrossRef\]](#) [\[PubMed\]](#)
26. Mishra, J.R.; Samal, S.K.; Mohanty, S.; Nayak, S.K. Polyvinylidene Fluoride (PVDF)/Ag@TiO<sub>2</sub> Nanocomposite Membrane with Enhanced Fouling Resistance and Antibacterial Performance. *Mater. Chem. Phys.* **2021**, *268*, 124723. [\[CrossRef\]](#)
27. Valenzuela, L.; Pedrosa, M.; Bahamonde, A.; Rosal, R.; Torres-Pinto, A.; Silva, C.G.; Faria, J.L.; Silva, A.M.T. Carbon Nitride—PVDF Photocatalytic Membranes for Visible-Light Degradation of Venlafaxine as Emerging Water Micropollutant. *Catal. Today* **2023**, *418*, 114042. [\[CrossRef\]](#)
28. Nieto-Sandoval, J.; Torres-Pinto, A.; Pedrosa, M.; Munoz, M.; De Pedro, Z.M.; Silva, C.G.; Faria, J.L.; Casas, J.A.; Silva, A.M.T. Application of g-C<sub>3</sub>N<sub>4</sub>-PVDF Membrane for the Photocatalytic Degradation of Micropollutants in Continuous Flow Mode: Impact of Water Matrix. *J. Environ. Chem. Eng.* **2023**, *11*, 110586. [\[CrossRef\]](#)
29. Zheng, X.; Liu, Y.; Liu, X.; Li, Q.; Zheng, Y. A Novel PVDF-TiO<sub>2</sub>@g-C<sub>3</sub>N<sub>4</sub> Composite Electrospun Fiber for Efficient Photocatalytic Degradation of Tetracycline under Visible Light Irradiation. *Ecotoxicol. Environ. Saf* **2021**, *210*, 111866. [\[CrossRef\]](#)
30. Huang, J.; Hu, J.; Shi, Y.; Zeng, G.; Cheng, W.; Yu, H.; Gu, Y.; Shi, L.; Yi, K. Evaluation of Self-Cleaning and Photocatalytic Properties of Modified g-C<sub>3</sub>N<sub>4</sub> Based PVDF Membranes Driven by Visible Light. *J. Colloid Interface Sci.* **2019**, *541*, 356–366. [\[CrossRef\]](#)
31. Sakarkar, S.; Muthukumaran, S.; Jegatheesan, V. Tailoring the Effects of Titanium Dioxide (TiO<sub>2</sub>) and Polyvinyl Alcohol (PVA) in the Separation and Antifouling Performance of Thin-Film Composite Polyvinylidene Fluoride (PVDF) Membrane. *Membranes* **2021**, *11*, 241. [\[CrossRef\]](#)
32. Dekkouche, S.; Morales-Torres, S.; Ribeiro, A.R.; Faria, J.L.; Fontàs, C.; Kebiche-Senhadj, O.; Silva, A.M.T. In Situ Growth and Crystallization of TiO<sub>2</sub> on Polymeric Membranes for the Photocatalytic Degradation of Diclofenac and 17 $\alpha$ -Ethinylestradiol. *Chem. Eng. J.* **2022**, *427*, 131476. [\[CrossRef\]](#)
33. Liu, S.; Véron, E.; Lotfi, S.; Fischer, K.; Schulze, A.; Schäfer, A.I. Poly(Vinylidene Fluoride) Membrane with Immobilized TiO<sub>2</sub> for Degradation of Steroid Hormone Micropollutants in a Photocatalytic Membrane Reactor. *J. Hazard. Mater.* **2023**, *447*, 130832. [\[CrossRef\]](#)
34. Wang, X.; Pehkonen, S.O.; Rämö, J.; Väänänen, M.; Highfield, J.G.; Laasonen, K. Experimental and Computational Studies of Nitrogen Doped Degussa P25 TiO<sub>2</sub>: Application to Visible-Light Driven Photo-Oxidation of As(III). *Catal. Sci. Technol.* **2012**, *2*, 784–793. [\[CrossRef\]](#)
35. Yadav, M.S.P.; Neghi, N.; Kumar, M.; Varghese, G.K. Photocatalytic-Oxidation and Photo-Persulfate-Oxidation of Sulfadiazine in a Laboratory-Scale Reactor: Analysis of Catalyst Support, Oxidant Dosage, Removal-Rate and Degradation Pathway. *J. Environ. Manag.* **2018**, *222*, 164–173. [\[CrossRef\]](#)
36. Chen, L.; Hou, Z.; Lu, X.; Chen, P.; Liu, Z.; Shen, L.; Bian, X.; Qin, Q. Antifouling Microfiltration Membranes Prepared from Poly(Vinylidene Fluoride)-Graft-Poly(N-Vinyl Pyrrolidone) Powders Synthesized via Pre-Irradiation Induced Graft Polymerization. *J. Appl. Polym. Sci.* **2013**, *128*, 3949–3956. [\[CrossRef\]](#)
37. Gao, Y.; Hu, M.; Mi, B. Membrane Surface Modification with TiO<sub>2</sub>-Graphene Oxide for Enhanced Photocatalytic Performance. *J. Memb. Sci.* **2014**, *455*, 349–356. [\[CrossRef\]](#)
38. Wang, J.; Wang, Y.; Zhu, J.; Zhang, Y.; Liu, J.; Van der Bruggen, B. Construction of TiO<sub>2</sub>@Graphene Oxide Incorporated Antifouling Nanofiltration Membrane with Elevated Filtration Performance. *J. Memb. Sci.* **2017**, *533*, 279–288. [\[CrossRef\]](#)
39. Méricq, J.P.; Mendret, J.; Brosillon, S.; Faur, C. High Performance PVDF-TiO<sub>2</sub> Membranes for Water Treatment. *Chem. Eng. Sci.* **2015**, *123*, 283–291. [\[CrossRef\]](#)
40. Medeiros, K.A.R.; Rangel, E.Q.; Sant’Anna, A.R.; Louzada, D.R.; Barbosa, C.R.H.; D’Almeida, J.R.M. Evaluation of the Electromechanical Behavior of Polyvinylidene Fluoride Used as a Component of Risers in the Offshore Oil Industry. *Oil Gas Sci. Technol. Rev. D’Ifp Energ. Nouv.* **2018**, *73*, 48. [\[CrossRef\]](#)
41. Cai, X.; Lei, T.; Sun, D.; Lin, L. A Critical Analysis of the  $\alpha$ ,  $\beta$  and  $\gamma$  Phases in Poly(Vinylidene Fluoride) Using FTIR. *RSC Adv.* **2017**, *7*, 15382–15389. [\[CrossRef\]](#)
42. Lanceros-Méndez, S.; Mano, J.F.; Costa, A.M.; Schmidt, V.H. FTIR and DSC Studies of Mechanically Deformed  $\beta$ -PVDF Films. *J. Macromol. Sci. Part B* **2001**, *40B*, 517–527. [\[CrossRef\]](#)
43. Boccaccio, T.; Bottino, A.; Capannelli, G.; Piaggio, P. Characterization of PVDF Membranes by Vibrational Spectroscopy. *J. Memb. Sci.* **2002**, *210*, 315–329. [\[CrossRef\]](#)

44. Peng, Y.; Wu, P. A Two Dimensional Infrared Correlation Spectroscopic Study on the Structure Changes of PVDF during the Melting Process. *Polymer* **2004**, *45*, 5295–5299. [\[CrossRef\]](#)
45. Koczkur, K.M.; Mourdikoudis, S.; Polavarapu, L.; Skrabalak, S.E. Polyvinylpyrrolidone (PVP) in Nanoparticle Synthesis. *Dalton Trans.* **2015**, *44*, 17883–17905. [\[CrossRef\]](#)
46. Martins, N.C.T.; Ângelo, J.; Girão, A.V.; Trindade, T.; Andrade, L.; Mendes, A. N-Doped Carbon Quantum Dots/TiO<sub>2</sub> Composite with Improved Photocatalytic Activity. *Appl. Catal. B* **2016**, *193*, 67–74. [\[CrossRef\]](#)
47. Sriwong, C.; Choojun, K.; Sriwong, S. High Photocatalytic Performance of 3D Porous-Structured TiO<sub>2</sub>@natural Rubber Hybrid Sheet on the Removal of Indigo Carmine Dye in Water. *SN Appl. Sci.* **2019**, *1*, 864. [\[CrossRef\]](#)
48. Mungondori, H.H.; Ramujana, S.; Katwire, D.M.; Taziwa, R.T. Synthesis of a Novel Visible Light Responsive  $\gamma$ -Fe<sub>2</sub>O<sub>3</sub>/SiO<sub>2</sub>/C-TiO<sub>2</sub> Magnetic Nanocomposite for Water Treatment. *Water Sci. Technol.* **2018**, *78*, 2500–2510. [\[CrossRef\]](#) [\[PubMed\]](#)
49. An, N.; Liu, H.; Ding, Y.; Lu, B.; Zhang, M. Fabrication of Micro-Structures on a PVDF/TiO<sub>2</sub> Nano-Composite Film Using Photocatalytic Lithography. *Appl. Surf. Sci.* **2012**, *258*, 5052–5055. [\[CrossRef\]](#)
50. Kaspar, P.; Sobola, D.; Částková, K.; Dallaev, R.; Šťastná, E.; Sedlák, P.; Knápek, A.; Trčka, T.; Holcman, V. Case Study of Polyvinylidene Fluoride Doping by Carbon Nanotubes. *Materials* **2021**, *14*, 1428. [\[CrossRef\]](#)
51. Chinh, V.D.; Broggi, A.; Di Palma, L.; Scarsella, M.; Speranza, G.; Vilardi, G.; Thang, P.N. XPS Spectra Analysis of Ti<sup>2+</sup>, Ti<sup>3+</sup> Ions and Dye Photodegradation Evaluation of Titania-Silica Mixed Oxide Nanoparticles. *J. Electron. Mater.* **2018**, *47*, 2215–2224. [\[CrossRef\]](#)
52. Li, W.; Li, H.; Zhang, Y.M. Preparation and Investigation of PVDF/PMMA/TiO<sub>2</sub> Composite Film. *J. Mater. Sci.* **2009**, *44*, 2977–2984. [\[CrossRef\]](#)
53. Tian, Z.; Song, Y.; Tao, K.; Liu, N.; Qin, S.; Yang, J.; Li, J.; Cui, Z. Preparation of TiO<sub>2</sub>-Ag Heterostructure via Tannic Acid-Assistance and Its Immobilization on PVDF Membrane for the Degradation of Dye under Visible Light. *Appl. Surf. Sci.* **2023**, *625*, 157195. [\[CrossRef\]](#)
54. Abdelmaksoud, M.; Mohamed, A.; Sayed, A.; Khairy, S. Physical Properties of PVDF-GO/Black-TiO<sub>2</sub> Nanofibers and Its Photocatalytic Degradation of Methylene Blue and Malachite Green Dyes. *Environ. Sci. Pollut. Res.* **2021**, *28*, 30613–30625. [\[CrossRef\]](#)
55. Makuła, P.; Pacia, M.; Macyk, W. How To Correctly Determine the Band Gap Energy of Modified Semiconductor Photocatalysts Based on UV-Vis Spectra. *J. Phys. Chem. Lett.* **2018**, *9*, 6814–6817. [\[CrossRef\]](#) [\[PubMed\]](#)
56. Liqiang, J.; Yichun, Q.; Baiqi, W.; Shudan, L.; Baojiang, J.; Libin, Y.; Wei, F.; Honggang, F.; Jiazhong, S. Review of Photoluminescence Performance of Nano-Sized Semiconductor Materials and Its Relationships with Photocatalytic Activity. *Sol. Energy Mater. Sol. Cells* **2006**, *90*, 1773–1787. [\[CrossRef\]](#)
57. Secondes, M.F.N.; Naddeo, V.; Belgiorio, V.; Ballesteros, F. Removal of Emerging Contaminants by Simultaneous Application of Membrane Ultrafiltration, Activated Carbon Adsorption, and Ultrasound Irradiation. *J. Hazard. Mater.* **2014**, *264*, 342–349. [\[CrossRef\]](#) [\[PubMed\]](#)
58. Lambropoulou, D.; Evgenidou, E.; Saliverou, V.; Kosma, C.; Konstantinou, I. Degradation of Venlafaxine Using TiO<sub>2</sub>/UV Process: Kinetic Studies, RSM Optimization, Identification of Transformation Products and Toxicity Evaluation. *J. Hazard. Mater.* **2017**, *323*, 513–526. [\[CrossRef\]](#)
59. Leyva, E.; Moctezuma, E.; López, M.; Baines, K.M.; Zermeño, B. Photocatalytic Degradation of  $\beta$ -Blockers in TiO<sub>2</sub> with Metoprolol as Model Compound. Intermediates and Total Reaction Mechanism. *Catal. Today* **2019**, *323*, 14–25. [\[CrossRef\]](#)
60. Abdullah, A.M.; Gracia-Pinilla, M.; Pillai, S.C.; O'Shea, K. UV and Visible Light-Driven Production of Hydroxyl Radicals by Reduced Forms of N, F, and P Codoped Titanium Dioxide. *Molecules* **2019**, *24*, 2147. [\[CrossRef\]](#)
61. Guo, Y.; Zhan, J.; Yu, G.; Wang, Y. Evaluation of the Concentration and Contribution of Superoxide Radical for Micropollutant Abatement during Ozonation. *Water Res.* **2021**, *194*, 116927. [\[CrossRef\]](#)
62. Kovácsa, K.; Tóth, T.; Wojnárovits, L. Evaluation of Advanced Oxidation Processes for  $\beta$ -Blockers Degradation: A Review. *Water Sci. Technol.* **2022**, *85*, 685–705. [\[CrossRef\]](#)
63. de Souza, L.P.; Sanches-Neto, F.O.; Junior, G.M.Y.; Ramos, B.; Lastre-Acosta, A.M.; Carvalho-Silva, V.H.; Teixeira, A.C.S.C. Photochemical Environmental Persistence of Venlafaxine in an Urban Water Reservoir: A Combined Experimental and Computational Investigation. *Process Saf. Environ. Prot.* **2022**, *166*, 478–490. [\[CrossRef\]](#)
64. Maximous, N.; Nakhla, G.; Wan, W. Comparative Assessment of Hydrophobic and Hydrophilic Membrane Fouling in Wastewater Applications. *J. Memb. Sci.* **2009**, *339*, 93–99. [\[CrossRef\]](#)
65. Alpatova, A.; Kim, E.-S.; Dong, S.; Sun, N.; Chelme-Ayala, P.; Gamal El-Din, M. Treatment of Oil Sands Process-Affected Water with Ceramic Ultrafiltration Membrane: Effects of Operating Conditions on Membrane Performance. *Sep. Purif. Technol.* **2014**, *122*, 170–182. [\[CrossRef\]](#)
66. García-Ivars, J.; Iborra-Clar, M.-I.I.; Alcaina-Miranda, M.I.M.-I.; Mendoza-Roca, J.-A.A.; Pastor-Alcañiz, L.; Garcia-Ivars, J.; Iborra-Clar, M.-I.I.; Alcaina-Miranda, M.I.M.-I.; Mendoza-Roca, J.-A.A.; Pastor-Alcañiz, L. Treatment of Table Olive Processing Wastewaters Using Novel Photomodified Ultrafiltration Membranes as First Step for Recovering Phenolic Compounds. *J. Hazard. Mater.* **2015**, *290*, 51–59. [\[CrossRef\]](#)
67. Acero, J.L.; Von Gunten, U. Influence of Carbonate on the Ozone/Hydrogen Peroxide Based Advanced Oxidation Process for Drinking Water Treatment. *Ozone Sci. Eng.* **2000**, *22*, 305–328. [\[CrossRef\]](#)



68. Chávez, A.M.; Solís, R.R.; Beltrán, F.J. Magnetic Graphene TiO<sub>2</sub>-Based Photocatalyst for the Removal of Pollutants of Emerging Concern in Water by Simulated Sunlight Aided Photocatalytic Ozonation. *Appl. Catal. B* **2020**, *262*, 118275. [[CrossRef](#)]
69. Vieira, O.; Ribeiro, R.S.; Pedrosa, M.; Lado Ribeiro, A.R.; Silva, A.M.T. Nitrogen-Doped Reduced Graphene Oxide—PVDF Nanocomposite Membrane for Persulfate Activation and Degradation of Water Organic Micropollutants. *Chem. Eng. J.* **2020**, *402*, 126117. [[CrossRef](#)]
70. American Public Health Association; American Water Works Association; Water Environment Federation. *Standard Methods for the Examination of Water and Wastewater*, 24th ed.; Lipps, W., Braun-Howland, E., Baxter, T., Eds.; APHA Press: Washington, DC, USA, 2023.

**Disclaimer/Publisher's Note:** The statements, opinions and data contained in all publications are solely those of the individual author(s) and contributor(s) and not of MDPI and/or the editor(s). MDPI and/or the editor(s) disclaim responsibility for any injury to people or property resulting from any ideas, methods, instructions or products referred to in the content.